



# PdCo alloys@N-doped porous carbon supported on reduced graphene oxide as a highly efficient electrocatalyst for hydrogen evolution reaction

Ming Zhong<sup>1</sup>, Lingling Li<sup>1</sup>, Kun Zhao<sup>1</sup>, Fangzhen He<sup>2</sup>, Bitao Su<sup>2,\*</sup> , and Dahui Wang<sup>1,\*</sup>

<sup>1</sup>State Key Laboratory of Advanced Processing and Recycling of Nonferrous Metal, Lanzhou University of Technology, Lanzhou 730050, People's Republic of China

<sup>2</sup>Laboratory of Eco-Functional Polymer Materials of the Ministry of Education, Key Laboratory of Eco-Environmental Polymer Materials of Gansu Province, College of Chemistry and Chemical Engineering, Northwest Normal University, Lanzhou 730070, People's Republic of China

**Received:** 23 January 2021

**Accepted:** 24 May 2021

**Published online:**

8 June 2021

© The Author(s), under exclusive licence to Springer Science+Business Media, LLC, part of Springer Nature 2021

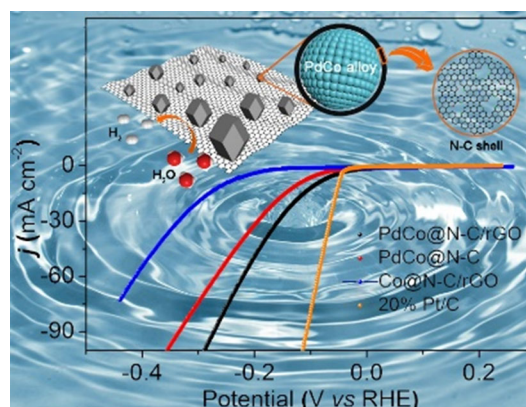
## ABSTRACT

Water splitting is considered as one of the recommendable techniques to realize clear and renewable hydrogen production. However, it suffers from lacking efficient and sustainable catalysts. Herein, a metal–organic framework/graphene oxide pyrolysis strategy was proposed to prepare nitrogen-doped porous carbon-stabilized alloys supported on reduced graphene oxide (PdCo@N–C/rGO) composite. When evaluated as an electrocatalyst for hydrogen evolution reaction (HER), the as-obtained PdCo@N–C/rGO shows an excellent performance in acidic media including positive onset potential close to that of commercial Pt/C (*vs.* SCE), low overpotential and Tafel slope, as well as long-term durability. Also, it delivers outstanding HER activities in alkaline and neutral conditions. The excellent performance could be mainly ascribed to their synergetic effect among alloy particles, nitrogen-doped porous carbon shell, and conductive rGO substrate.

Handling Editor: Kyle Brinkman.

Address correspondence to E-mail: subt0608@163.com; wangdh@lut.edu.cn

## GRAPHICAL ABSTRACT



A metal-organic framework engineered strategy was proposed to prepare N-doped porous carbon-stabilized PdCo alloys supported on reduced graphene oxide nanocomposite. Specifically, the as-obtained catalyst delivers excellent electrochemical activity for hydrogen evolution reaction.

## Introduction

The increasing concerns on fossil fuel consumption and environmental problems call for clean and renewable energy sources [1, 2]. Hydrogen energy has received a broad attention and been identified as a desirable alternative to non-fossil fuel resource due to the advantages of high energy density, zero-emission, and abundant resource [3]. Recently, water splitting with high energy conversion and storage efficiency is used as an efficient and environmental technology to produce high-pure hydrogen [4–8]. However, its high overpotential cannot meet the requirement of anodic hydrogen evolution reaction (HER). Traditional noble metal-based catalysts exhibit negligible overpotential and outstanding durability but suffer from high cost and limited abundance, thereby hindering their large-scale industrial application [9–13]. This evokes a widespread search for non-noble metal-based alternatives, such as Co- [14], Ni- [15, 16], and Mo-based catalysts [17–21]. Particularly, Co-based catalysts serve as excellent examples of novel electrocatalysts for HER [3, 22].

Recent years have witnessed the rapid development of Co-based catalysts in HER [23, 24]. Originally, cobaloxime and diimine-dioxime compounds were reported by Artero et al., which showed a low overpotential for proton reduction when evaluated as molecular electrocatalysts for hydrogen evolution [25–27]. However, harsh synthesis condition significantly hinders their practical application. To address this issue, various Co-based catalysts, such as CoO [28], CoSe<sub>2</sub> [29–32], CoP [33–36], CoPS [37, 38], Co<sub>2</sub>B [39], CuCo [40], and FeCo [41], have sprung up owing to simple preparation process, low cost, and excellent HER activity as well as durability relative to those Co-based complexes [42]. Nonetheless, most of them exhibit inferior electrocatalytic activities to platinum-based catalysts in overpotential and durability. Therefore, Co-based catalysts are still unable to substitute Pt-based catalysts in the short term.

Bimetallic catalysts combining platinum group elements with Co commonly deliver superior catalytic performance via cooperative interaction, which are not observable by their individual monometallic counterparts [3, 43–46]. Theoretical and experimental results have proved that alloying platinum group elements with Co could change the average energy of surface d-band and the width of d-band originated

from cumulative strain and ligand effect. This can result in modification of the surface chemical properties and remarkably promote the HER activity [3, 43, 47, 48]. Among them, palladium has been considered to form alloy due to its higher affinity for hydrogen and relatively cheaper price than platinum [2]. In addition, integrating alloy with carbon substrates, especially encapsulating them in heteroatom-doped carbon, can enhance HER performance [43]. Despite of great advantages, the complex preparation procedure for most materials makes it urgent to search for relatively simple and effective approaches to realize the encapsulation of alloy in carbon layers.

Metal–organic frameworks (MOFs), a class of novel crystalline material assembled through coordination interaction between metal ions/clusters and organic linkers, have proved to be potential precursors to synthesize heteroatom-doped porous carbon stabilized metal/metal compounds for HER. The as-formed materials preserve metal source, abundant carbon and heteroatom species, high surface area, tunable porosity, and well-organized nanostructure [39, 49–55]. To date, RuCo-based catalysts [3] and PtCo-based catalysts [45] have been synthesized by using noble metal-doped MOFs as precursors. However, choosing Pd-doped MOFs as precursors to synthesize PdCo alloys wrapped in N-doped porous carbon was just reported by Chen et al. [43]. The as-prepared catalyst delivers remarkable HER activity with low overpotential and Tafel slope as well as excellent cycle stability in 0.5 M H<sub>2</sub>SO<sub>4</sub> media than that of Co wrapped N-doped porous carbon. Therefore, it can be estimated that MOFs can be pyrolyzed to obtain the composites consisting of heteroatom-doped porous carbon and nanosized alloys through introducing noble metals into MOFs.

In this work, we take a facile MOF-assisted strategy to synthesize a new kind of composite consisting of PdCo alloy nanoparticles encapsulated with N-doped porous carbon and reduced graphene oxide substrates (denoted as PdCo@N-C/rGO) by pyrolyzing Pd-incorporated ZIF-67/GO precursors under N<sub>2</sub> atmosphere. The carbon shell effectively stabilizes PdCo alloys and prevents them from aggregation and corrosion during HER process. Meanwhile, rGO sheets provide ideal substrates for electrocatalysts due to their large surface area, good conductivity, and high stability. Benefiting from the synergistic effect of the PdCo alloy, N-doped porous carbon, and rGO components, the as-synthesized PdCo@N-C/

rGO material exhibits outstanding HER performance in acidic, alkaline, and neutral conditions.

## Experimental

### Chemicals

All the reagents and solvents, including graphene oxide (GO, XFNANO Materials Tech Co., Ltd, Nanjing), sodium chloropalladite (AR, Aladdin), L-ascorbic acid (AR, > 99.0%, Aladdin), polyvinylpyrrolidone (PVP, *M* = 24,000, Aladdin), potassium chloride (KCl, Bodi Chemicals, Tianjin), potassium bromide (KBr, Regent Chemical, Tianjin), cobalt nitrate hexahydrate (Co(NO<sub>3</sub>)<sub>2</sub>·6H<sub>2</sub>O, AR, Aladdin), 2-methylimidazole (AR, Aladdin), methanol (CH<sub>3</sub>OH, 99.5%, Hengshan Chemicals, Tianjin), and distilled water were commercially obtained and used without further purification.

### Preparation of Pd nanoparticles

Pd nanoparticles were prepared by following the reported procedure [56]. Briefly, an aqueous solution (8 mL) of PVP (105 mg), L-ascorbic acid (60 mg), KCl (185 mg), and KBr (5 mg) was added into an aqueous solution (3 mL) of sodium chloropalladite (57 mg). The mixture was stirred for 10 min and then agitated vigorously at 80 °C for 3 h. After cooling down to room temperature, the resultant black precipitate was separated by diethyl ether and then was dispersed in methanol (8 mL) for further use.

### Preparation of Pd-ZIF-67/GO

In a typical procedure, 2 ml of methanol solution of Pd was firstly mixed with 30 mL of methanol solution of GO (1 mg mL<sup>-1</sup>). Then, 50 mL of methanol solution of 2-methylimidazole (0.5820 g) was added into the above mixture with continuous stirring for 1 h followed by quick pour of a 50 mL of methanol solution of Co(NO<sub>3</sub>)<sub>2</sub>·6H<sub>2</sub>O (0.6562 g). Finally, the mixture was kept undisturbed for 24 h. The resultant composite was collected by centrifugation, washed with methanol for at least five times, and then dried at 60 °C for 12 h. The as-obtained sample was denoted as Pd-ZIF-67/GO.

## Preparation of PdCo@N-C/rGO

The as-synthesized Pd-ZIF-67/GO precursors were transferred into a tube furnace and maintained 350 °C for 1.5 h. Following, the pyrolysis temperature was further raised to 900 °C at a ramp rate of 5 °C min<sup>-1</sup> and kept for 3.5 h under a nitrogen atmosphere. After cooling down to room temperature, the PdCo@N-C/rGO sample was collected and stored. By comparison, Co@N-C/rGO and PdCo@N-C samples were also prepared by pyrolysis of ZIF-67/GO and Pd-ZIF-67 precursors under the same conditions, respectively.

## Material characterization

Power X-ray diffraction (PXRD) patterns were recorded in the range of 3–80° by step scanning with a Rigaku Mini Flex600 X-ray diffraction meter at 40 kV, 15 mA with a Cu-target tube. The morphology of samples was characterized by field emission scanning electron microscopy (FESEM, JEOL JSM-7500F), transmission electron microscope (TEM), high-resolution transmission electron microscopy (HRTEM), and energy-dispersive X-ray (EDX) (JEOL, JEM-1200EX, 20–120 kV). X-ray photoelectron spectroscopy (XPS) was operated on a Thermo Scientific ESCALAB 250Xi Versaprobe system. Inductively coupled plasma (ICP, Thermo Electron Corporation, X7) and elemental analysis (Vario EL cube) were used to quantitatively confirm the content of each element. Raman spectra were collected on a RTS-HiR-AM with Raman Laser source of 532 nm. Nitrogen adsorption-desorption measurement was performed on an ASAP 2020 (Micromeritics) at 77 K, and the BET method was utilized to calculate the specific surface areas ( $S_{\text{BET}}$ ). Pore size distribution was calculated based on Density Functional Theory (DFT) using the data from the adsorption branch.

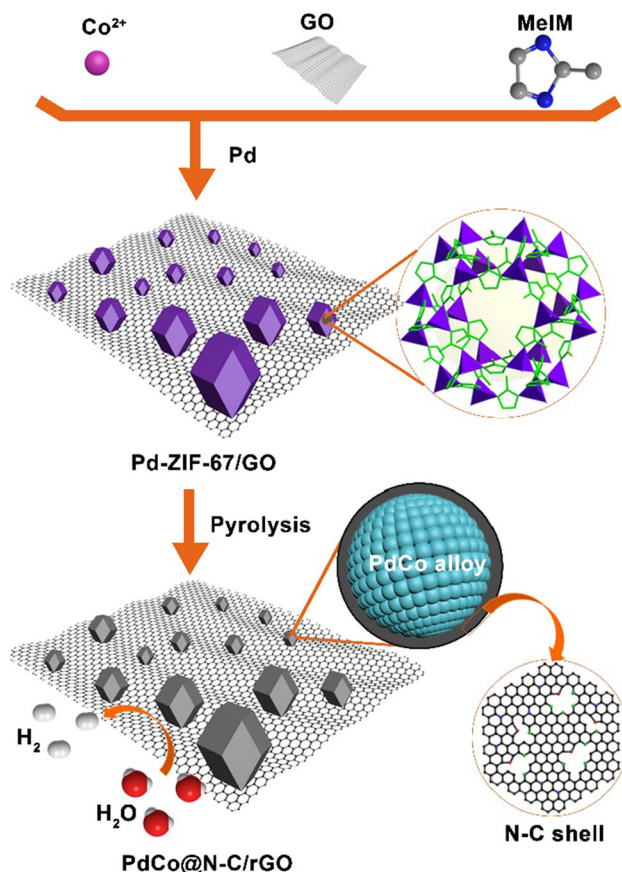
## Electrochemical HER measurement

All the electrochemical HER measurements were performed in a standard three-electrode system on a CHI760E electrochemical workstation (Shanghai Chenhua Co., China) in 0.5 M H<sub>2</sub>SO<sub>4</sub>, 1.0 M KOH, and 1.0 M KHCO<sub>3</sub> solutions. The working electrodes were prepared as follows: 5 mg of catalyst and 20 μL of 5 wt% Nafion solution were ultrasonically dispersed in 280 μL of ethanol/water mixed solvent (9:5

v/v) for at least 1 h to form a homogeneous ink. Then, 5 μL of catalyst ink (catalyst loading: ca. 0.66 mg cm<sup>-2</sup>) was loaded onto the glassy carbon electrode surface and then dried for measurement. Prior to HER measurements, the electrolyte was bubbled with N<sub>2</sub>. All of the potentials were calibrated to a RHE. The HER polarization curves were measured with a scan rate of 5.0 mV s<sup>-1</sup>. Tafel slope was obtained by plotting overpotential against the logarithm of current density (log |*J*|). Chronoamperometry measurement was performed to evaluate the long-term durability. To estimate the electro-chemical active surface area of catalyst, the HER cyclic voltammograms were obtained by ranging potential from -0.25 to -0.15 V (vs. SCE, in 0.5 M H<sub>2</sub>SO<sub>4</sub>) with various scan rates of 10, 20, 40, 60, 80, 100, 120, 140, 160, 180, and 200 mV s<sup>-1</sup>. By plotting the  $\Delta j = j_a - j_c$  against the CV scan rate, the linear slope that is twice of the double layer capacitance ( $C_{\text{dl}}$ ) is used to represent electrochemical active surface area (ECSA).

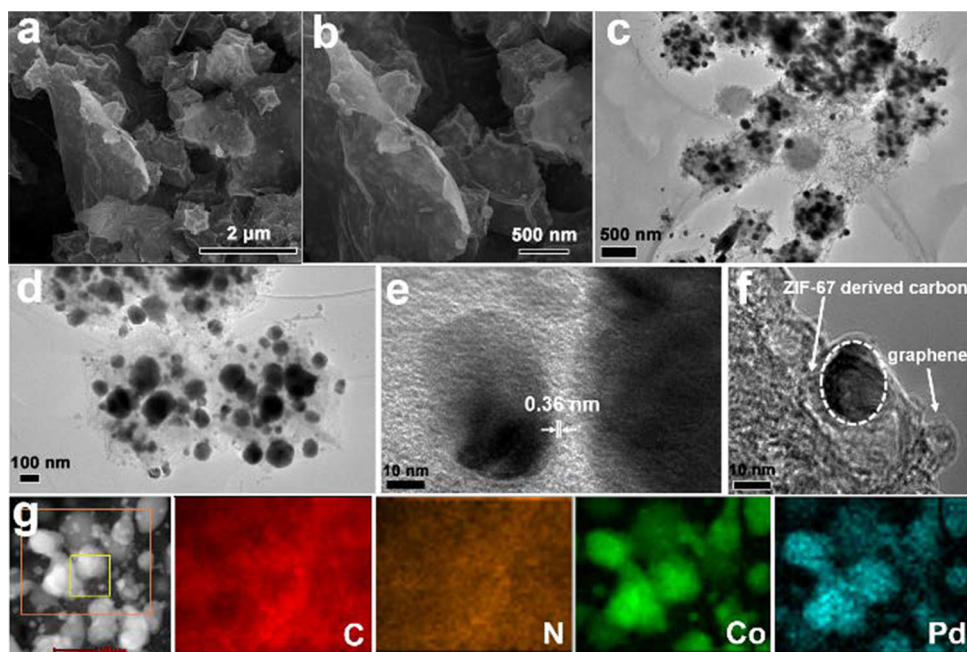
## Results and discussion

The general synthesis process of PdCo alloy-encapsulated N-doped porous carbon supported on rGO substrate is presented in Scheme 1. Firstly, Pd-ZIF-67/GO precursor was prepared by using Pd nanoparticles, Co(NO<sub>3</sub>)<sub>2</sub>·6H<sub>2</sub>O, methylimidazole (MeIm), and graphene oxide (GO) as starting materials. The power X-ray diffraction (PXRD) patterns unambiguously reveal the successful preparation of Pd-ZIF-67/GO. All peaks are in good agreement with simulated ZIF-67 and Pd (card: JCPDS no. 65–6174), as shown in Figure S1 (Supporting Information). The field-emission scanning electron microscopy (FESEM) images show that Pd-incorporated ZIF-67 microcrystal is nearly rhombic and supported onto GO substrate, as shown in Figure S2 (Supporting Information). Subsequently, Pd-ZIF-67/GO precursors were pyrolyzed at 350 °C followed by 900 °C in N<sub>2</sub> atmosphere, resulting in the formation of PdCo@N-C/rGO material. At a low annealing temperature, the solvent molecules can escape from the precursor to form abundant micropores and mesopores. During the high carbonization temperature, PdCo alloy could be encapsulated by N-doped carbon derived from ligands, and GO sheets were simultaneously reduced to rGO. The rGO not only ensures good electrical conductivity but also acts as a



**Scheme 1** Schematic illustration for the synthetic process of PdCo@N-C/rGO material.

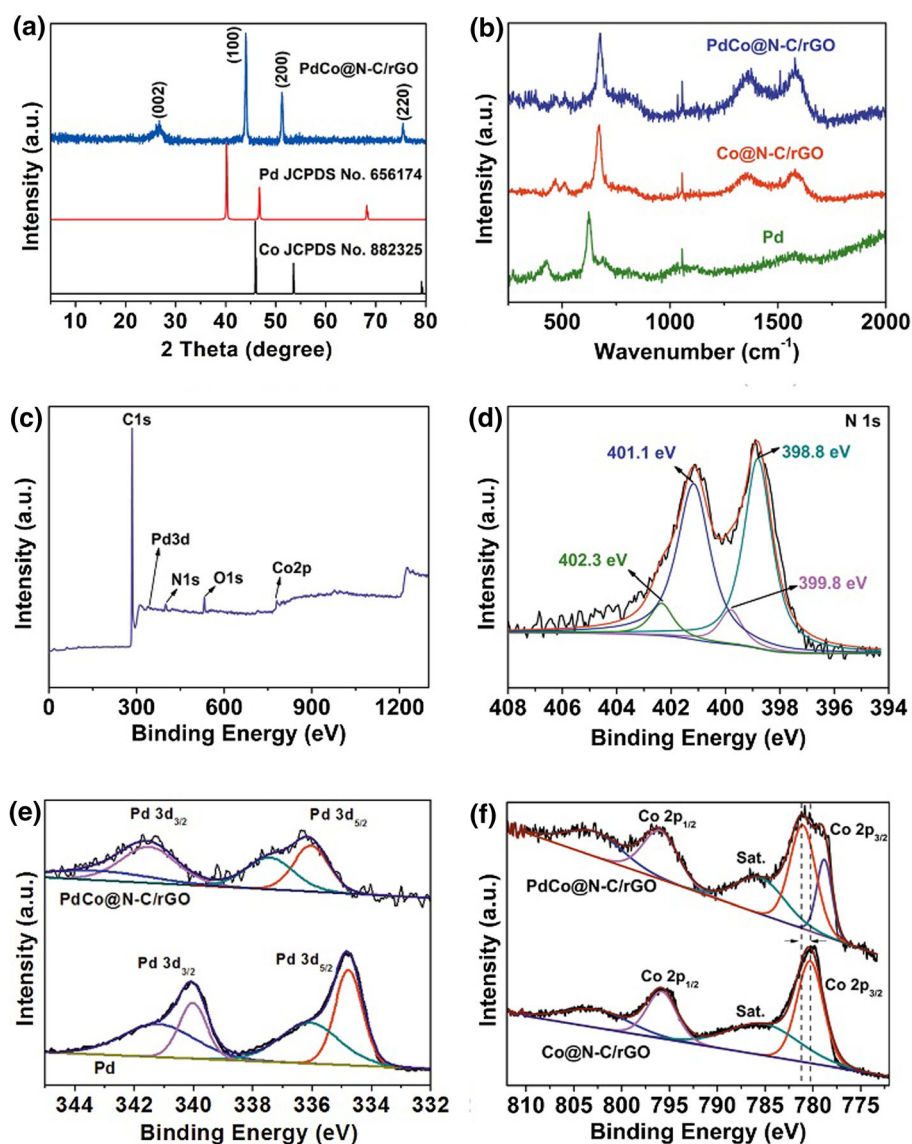
**Figure 1** (a, b) SEM, (c, d, e) TEM, (f) HRTEM images, and (g) TEM image with corresponding elemental mapping of C, N, Co, and Pd of as-synthesized PdCo@N-C/rGO composite.



substrate to make ZIF-67-derived N-doped carbon uniformly loaded [57].

The morphology and phase characteristics of PdCo@N-C/rGO composite were primarily examined by FESEM and transmission electron microscopy (TEM). As shown in Fig. 1a, b, the general morphology of PdCo@N-C/rGO is different from the original ones after thermal treatment. The rGO sheets show a shrunk and crinkled structure, while Pd-incorporated ZIF-67 octahedrons become rough and are dispersed on rGO sheets uniformly (Fig. 1c, d). At this point, PdCo alloy nanoparticles are formed. The size distribution of PdCo nanoparticles mainly ranges from 20 to 80 nm. The high-resolution TEM (HRTEM) images demonstrate that PdCo nanoparticles are encapsulated by ZIF-derived carbon shell (Fig. 1e, f). The surface element mapping result unambiguously verifies that PdCo@N-C/rGO is composed of Pd, Co, N, and C elements and they are homogeneously distributed (Fig. 1g). The BET surface area and pore size distribution characteristics of as-prepared PdCo@N-C/rGO and Co@N-C/rGO samples were examined by nitrogen adsorption/desorption measurement. The isotherm of PdCo@N-C/rGO exhibits typical microporous and mesoporous characteristics with a type-IV curve. The Brunauer–Emmett–Teller (BET) surface area is

**Figure 2** **a** XRD pattern of as-prepared PdCo@N-C/rGO; **b** Raman spectra of PdCo@N-C/rGO, Co@N-C/rGO and Pd samples; **c** XPS spectrum; and **d** high resolution N 1 s spectrum of PdCo@N-C/rGO sample; **e** high-resolution Pd 3d and **f** Co 2p spectra of PdCo@N-C/rGO, Co@N-C/rGO and Pd samples.



$245.9 \text{ m}^2 \text{ g}^{-1}$ , which is near to that of Co@N-C/rGO ( $224.9 \text{ m}^2 \text{ g}^{-1}$ ), indicating that the introduction of Pd has a little impact on the surface area (Figure S3, Supporting Information). According to inductively coupled plasma optical emission spectrometry (ICP-OES) analysis, the weight contents of Pd and Co for PdCo@N-C/rGO were determined to be 2.0% and 29.8%, respectively.

The PXRD pattern reveals the phase component of PdCo@N-C/rGO. As shown in Fig. 2a, a broad peak at  $26.5^\circ$  ( $2\theta$ ) is assigned to a characteristic of graphite carbon (002) peak with good graphitization. In addition, the PdCo@N-C/rGO presents three peaks at  $43.6^\circ$ ,  $50.5^\circ$ , and  $74.7^\circ$  ( $2\theta$ ), which are typically assigned to (111), (200), and (220) of cobalt palladium

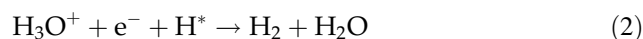
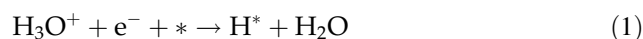
in Fm-3 m cubic system (JCPDS: no. 65–6174). Compared with simulated PXRD patterns of cobalt (JCPDS: no. 88–2325) and Palladium (JCPDS: no. 65–6174), the peak locations of PdCo@N-C/rGO shift, indicating that Pd is successfully incorporated into the Co cubic structure to form an alloy phase [58, 59]. The structural feature of the carbonized samples was also characterized by Raman spectroscopy. As shown in Fig. 2b, PdCo@N-C/rGO shows a slight peak-shift at ca.  $670 \text{ cm}^{-1}$  compared with Pd or Co@N-C/rGO, indicating the existence of strong interaction between Pd and Co, which is in accordance with PXRD results. Meanwhile, two characteristic peaks at  $1357 \text{ cm}^{-1}$  and  $1578 \text{ cm}^{-1}$  correspond to typical D and G bands of PdCo@N-C/

rGO, which represent characteristic features of disordered and graphitic carbon, respectively [57]. The  $I_D/I_G$  ratio is ca. 0.86, indicating a high graphitization degree. This is ascribed to the introduction of rGO component. X-ray photoelectron spectroscopy (XPS) was employed to investigate the chemical state and effect of Pd on electron structure of Co. As shown in Fig. 2c, the full XPS spectrum confirms the existence of Pd, Co, C, and N, which is in good accordance with energy-dispersive X-ray (EDX) elemental mapping result. In high-resolution N1s spectrum of PdCo@N-C/rGO, two obvious peaks are deconvoluted into four individual peaks with binding energies at 398.8, 399.8, 401.1, and 402.2 eV, which are assigned to pyridinic-N, pyrrolic-N-metal, pyrrolic-N, and quaternary-N, respectively [3, 60]. In high-resolution Pd 3d spectra (Fig. 2e), both Pd 3d<sub>5/2</sub> and 3d<sub>3/2</sub> peaks of PdCo@N-C/rGO positively shift to higher binding energies compared with Pd, indicating the existence of chemical interaction between Pd and Co in PdCo@N-C/rGO [61]. The binding energy in PdCo@N-C/rGO could originate from the d-band hybridization between metal atoms upon alloying owing to the fact that stronger bonds can be formed in the d-orbital, which thus reduces the ability to form strong bonds with adsorbed reactants [62]. Similarly, the high-resolution Co2p spectra of PdCo@N-C/rGO and Co@N-C/rGO are presented in Fig. 2f. Each Co2p peak can be resolved into two pairs of doublets, and two obvious Co<sup>0</sup> and Co<sup>II</sup> species peaks, indicating the existed Co<sup>II</sup> comes from surface oxidation of metallic Co [3]. In addition, both Co 2p<sub>3/2</sub> and 2p<sub>1/2</sub> peaks of PdCo@N-C/rGO shift to higher binding energies relative to the Co 2p<sub>3/2</sub> and 2p<sub>1/2</sub> peaks of Co@N-C/rGO, further demonstrating the strong electron interaction between Pd and Co, which probably facilitates the electrocatalytic activity and durability for HER.

Intrigued by the structural and component features, PdCo@N-C/rGO composite was evaluated as an electrocatalyst for HER in 0.5 M H<sub>2</sub>SO<sub>4</sub> electrolyte by using a typical three-electrode electrochemical system. By comparison of HER performance, Pd-ZIF-67 and ZIF-67/GO were prepared and went through the same treatment. The final products were denoted as PdCo@N-C and Co@N-C/rGO (the structures and morphologies were confirmed by XRD and TEM technique as shown in Figures S4 and S5, Supporting Information). The electrocatalytic performance was firstly evaluated by an overpotential value versus

reversible hydrogen electrode (RHE) at 10 mA cm<sup>-2</sup>, which is considered to reach 12.3% efficient solar water-splitting device at this current density [3, 63]. Figure 3a presents the polarization curves of samples with a scan rate of 5 mV s<sup>-1</sup>. Observably, PdCo@N-C/rGO exhibits more positive onset potential than Co@N-C/rGO, which is near to the thermodynamic potential of H<sub>2</sub> evolution. In addition, the overpotential value of PdCo@N-C/rGO is measured to be 87 mV at a current density of 10 mA cm<sup>-2</sup>, which is close to the value of commercial Pt/C catalyst (49 mV) among these samples. Obviously, the overpotential of PdCo@N-C/rGO is lower than that of PdCo@N-C (122 mV) and Co@N-C/rGO (252 mV). It indicates that PdCo alloy, N-doped porous carbon, and rGO play indispensable roles in the improvement in electrochemical performance for HER.

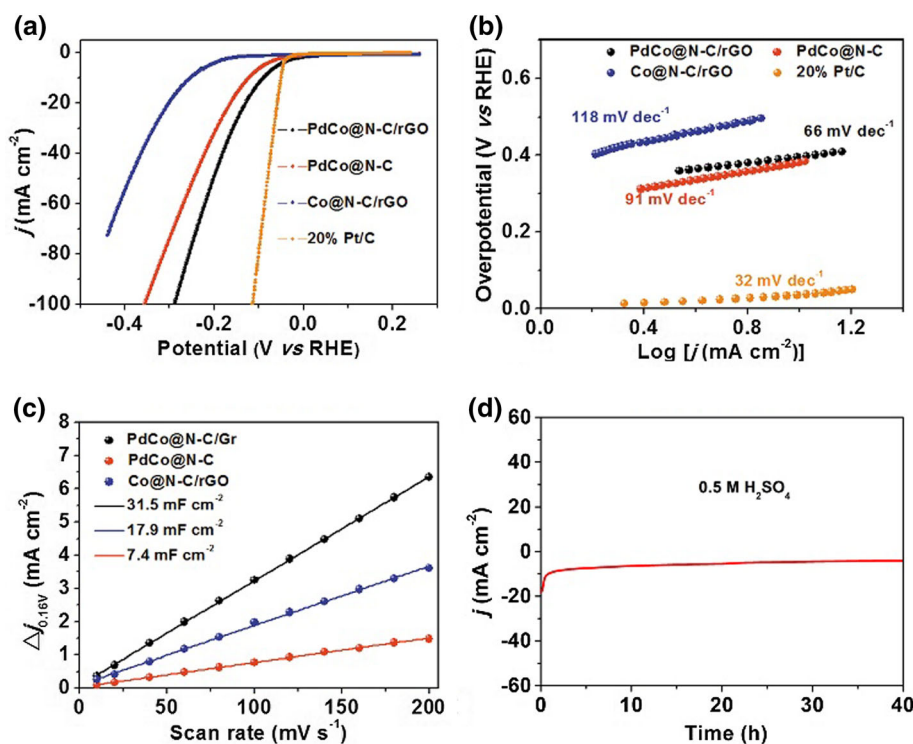
Subsequently, the corresponding kinetics of the above-mentioned catalysts were evaluated by Tafel plots measured in a 0.5 M H<sub>2</sub>SO<sub>4</sub> electrolyte. Typically, the hydrogen evolution mechanism in acidic electrolyte mainly contains three principal steps including the Volmer (Eq. 1), the Heyrovsky (Eq. 2), and the Tafel step (Eq. 3) [56], as listed as follows:



As shown in Fig. 3b, the Tafel slope of commercial Pt/C (32 mV dec<sup>-1</sup>) demonstrates that the typical Volmer-Tafel mechanism happened. Under the same conditions, the PdCo@N-C/rGO catalyst presents a Tafel slope value of 66 mV dec<sup>-1</sup>, which demonstrates a Volmer-Heyrovsky mechanism occurred in hydrogen evolution process of PdCo@N-C/rGO [1, 58]. Moreover, the Tafel slope of PdCo@N-C/rGO is smaller than that of PdCo@N-C and Co@N-C/rGO (91 and 118 mV dec<sup>-1</sup>), and this value is better than most of those reported Co-based catalysts (Table S1, Supporting Information). The reason could be ascribed to the smaller electron transport barrier for PdCo@N-C/rGO, in which PdCo alloy core can transfer more number of electrons to the nitrogen-doped carbon shell and graphene than pure metal core in order to enhance C-H bond, which will decline free energy  $\Delta G_{\text{H}^*}$  and thereby enhance the electrocatalytic activity [3].

The electrochemical active surface areas of PdCo@N-C/rGO, PdCo@N-C, and Co@N-C/rGO

**Figure 3** (a) Polarization curves and (b) Tafel plots of PdCo@N-C/rGO, PdCo@N-C, Co@N-C/rGO, and commercial Pt/C in 0.5 M H<sub>2</sub>SO<sub>4</sub>; (c) estimation of  $C_{dl}$  by plotting the current density variation (160 mV *vs.* RHE); (d) chronoamperometric curve ( $i$  *vs.*  $t$ ) of PdCo@N-C/rGO at an applied potential of  $-0.158$  V (*vs.* RHE).



were evaluated by electrochemical double-layer capacitance ( $C_{dl}$ ) (Fig. 3c). The  $C_{dl}$  was simulated by using a cyclic voltammetry (CV) method (Figure S6, Supporting Information). The results show that the  $C_{dl}$  of PdCo@N-C/rGO is much higher than that of Co@N-C/rGO and PdCo@N-C, implying the abundant electrochemical active surface area on PdCo@N-C/rGO catalyst. Such an increase in  $C_{dl}$  endows PdCo@N-C/rGO with excellent HER activity. Electrochemical impedance spectroscopy (EIS) was conducted to further explain the enhanced performance of PdCo@N-C/rGO, and corresponding Nyquist plots of three catalysts are shown in Figure S7. Commonly, the semicircle in low frequency region is related to the charge-transfer resistance ( $R_{ct}$ ). As can be seen, PdCo@N-C/rGO exhibits smaller diameter than that of Co@N-C/rGO and PdCo@N-C, indicating smaller  $R_{ct}$  and easier electron transfer in PdCo@N-C/rGO electrode, which thus contributes to highly electrochemical activity. In addition, the stability of PdCo@N-C/rGO catalyst was evaluated by Chronoamperometry (CA) test and TEM characterization after cycling. As shown in Fig. 3d, the catalytic activity shows a slight reduction over 40 h at a catalytic current of nearly  $10 \text{ mA cm}^{-2}$  with an applied potential of  $-0.158$  V (*vs.* RHE), demonstrating its good durability in acidic electrolyte. The

morphology of PdCo@N-C/rGO after cycling was well preserved with the initial morphology, and the EDX mapping presents the uniform distribution of C, N, Co, and Pd elements (Figure S8, Supporting Information), indicating its structural stability.

Combining the low overpotential, small Tafel slope, and good durability of PdCo@N-C/rGO, the improved catalytic performance could be attributed to the synergistic effect among PdCo alloys, N-doped porous carbon shell, and rGO substrate. Firstly, rGO substrate offers good conductivity and large surface area to facilitate mass diffusion and electron transport on PdCo@N-C/rGO catalyst. Secondly, PdCo alloy nanoparticles provide more active sites to enhance quick adsorption and desorption of H<sub>2</sub> in acidic electrolyte. Thirdly, ZIFs-derived N-doped porous carbon shells make PdCo nanoparticles disperse uniformly and prevent them from corrosion, which are beneficial for enhanced stability and durability of PdCo@N-C/rGO in acidic system [1].

In addition, the electrocatalytic performance of obtained catalysts was also investigated in alkaline and neutral media. Similarly, the PdCo@N-C/rGO catalyst exhibits the lowest overpotential and smallest Tafel slope than that of PdCo@N-C and Co@N-C/rGO with the values of 251 mV, 149 mV  $\text{dec}^{-1}$  in 1.0 M KOH (Figure S9a, S9b) and 115 mV, 41 mV



$\text{dec}^{-1}$  in 1.0 M  $\text{KHCO}_3$  (Figure S9d, S9e). In addition, EIS analysis also verifies that PdCo@N-C/rGO possesses the lowest charge transfer resistance than Co@N-C/rGO and PdCo@N-C (Figure S9c, S9f), corroborating the high HER performance of PdCo@N-C/rGO.

## Conclusion

In summary, a PdCo@N-C/rGO composite was successfully prepared through one-step pyrolysis of Pd-incorporated ZIF-67/GO precursor and applied as an electrocatalyst in HER. The synergetic effect among PdCo alloy, N-doped porous carbon shell, and electrochemically conductive rGO support endows the as-made PdCo@N-C/rGO catalyst with excellent HER performance in acidic, alkaline, and neutral electrolytes, including low overpotential (87, 251, 115 mV at 10 mA  $\text{cm}^{-2}$ ), small Tafel slope (66, 150, 41 mV  $\text{dec}^{-1}$ ), and long-term durability. Meanwhile, the PdCo@N-C/rGO catalyst shows advantages over PdCo@N-C and Co@N-C/rGO, respectively. This work might bring new opportunities to develop alloy-based HER catalysts via MOF pyrolysis strategy.

## Acknowledgements

This work was supported by the open fund of the State Key Laboratory of Advanced Processing and Recycling of Nonferrous Metals (SKLAB02019006) and the Youth Scientific and Technical Plan Project of Gansu Province (20JR10RA198).

## Declarations

**Conflict of interest** The authors declare that they have no known competing financial interests or personal relationships that could have appeared to influence the work reported in this paper.

**Supplementary Information:** The online version contains supplementary material available at <http://doi.org/10.1007/s10853-021-06212-6>.

## References

- [1] Tang YJ, Gao MR, Liu CH et al (2015) Porous molybdenum-based hybrid catalysts for highly efficient hydrogen evolution. *Angew Chem Int Ed* 54:12928–12932. <https://doi.org/10.1002/anie.201505691>
- [2] Chen A, Ostrom C (2015) Palladium-based nanomaterials: synthesis and electrochemical applications. *Chem Rev* 115:11999–12044. <https://doi.org/10.1021/acs.chemrev.5b00324>
- [3] Su J, Yang Y, Xia G, Chen J, Jiang P, Chen Q (2017) Ruthenium-cobalt nanoalloys encapsulated in nitrogen-doped graphene as active electrocatalysts for producing hydrogen in alkaline media. *Nat Commun* 8:14969. <https://doi.org/10.1038/ncomms14969>
- [4] Zhang R, Wang X, Yu S et al (2017) Ternary  $\text{NiCo}_2\text{P}_x$  nanowires as pH-universal electrocatalysts for highly efficient hydrogen evolution reaction. *Adv Mater* 29:1605502. <https://doi.org/10.1002/adma.201605502>
- [5] Walter MG, Warren EL, McKone JR, Boettcher SW, Mi Q, Santori EA, Lewis NS (2010) Solar water splitting cells. *Chem Rev* 110:6446–6473. <https://doi.org/10.1021/cr1002326>
- [6] Wang J, Cui W, Liu Q, Xing Z, Asiri AM, Sun X (2016) Recent progress in cobalt-based heterogeneous catalysts for electrochemical water splitting. *Adv Mater* 28:215–230. <https://doi.org/10.1002/adma.201502696>
- [7] James MI (2016) Recent progress on earth abundant hydrogen evolution reaction and oxygen evolution reaction bifunctional electrocatalyst for overall water splitting in alkaline media. *J Power Sour* 333:213–236. <https://doi.org/10.1016/j.jpowsour.2016.09.161>
- [8] McKone JR, Marinescu SC, Brunshwig BS, Winkler JR, Gray HB (2014) Earth-abundant hydrogen evolution electrocatalysts. *Chem Sci* 5:865–878. <https://doi.org/10.1039/c3sc51711j>
- [9] Wang Y-J, Wilkinson DP, Zhang J (2011) Noncarbon support materials for polymer electrolyte membrane fuel cell electrocatalysts. *Chem Rev* 111:7625–7651. <https://doi.org/10.1021/cr100060r>
- [10] Mahmood A, Guo W, Tabassum H, Zou R (2016) Metal-organic framework-based nanomaterials for electrocatalysis. *Adv Energy Mater* 6:1600423. <https://doi.org/10.1002/aenm.201600423>
- [11] Safizadeh F, Ghali E, Houlachi G (2015) Electrocatalysis developments for hydrogen evolution reaction in alkaline solutions - a Review. *Int J Hydrogen Energy* 40:256–274. <https://doi.org/10.1016/j.ijhydene.2014.10.109>
- [12] Seh ZW, Kibsgaard J, Dickens CF, Chorkendorff I, Nørskov JK, Jaramillo TF (2017) Combining theory and experiment

- in electrocatalysis: insights into materials design. *Science*. <https://doi.org/10.1126/science.aad4998>
- [13] Hou Y, Pang H, Xin J, Ma H, Li B, Wang X, Tan L (2020) Multi-interface-modulated  $\text{CoS}_2/\text{MoS}_2$  nanoarrays derived by pre-designed germanomolybdate polymer showing ultra-highly electrocatalytic activity for hydrogen evolution reaction in wide pH range. *Adv Mater Interfaces* 7:2000780. <https://doi.org/10.1002/admi.202000780>
- [14] Hu X, Zhang S, Sun J et al (2019) 2D Fe-containing cobalt phosphide/cobalt oxide lateral heterostructure with enhanced activity for oxygen evolution reaction. *Nano Energy* 56:109–117. <https://doi.org/10.1016/j.nanoen.2018.11.047>
- [15] Jiao Y, Hong W, Li P, Wang L, Chen G (2019) Metal-organic framework derived Ni/NiO micro-particles with subtle lattice distortions for high-performance electrocatalyst and super-capacitor. *Appl Catal B* 244:732–739. <https://doi.org/10.1016/j.apcatb.2018.11.035>
- [16] Wang C-P, Kong L-J, Sun H et al (2019) Carbon layer coated  $\text{Ni}_3\text{S}_2/\text{MoS}_2$  nanohybrids as efficient bifunctional electrocatalysts for overall water splitting. *Chem ElectroChem* 6:5603–5609. <https://doi.org/10.1002/celec.201901767>
- [17] Gao B, Du X, Ma Y et al (2020) 3D flower-like defected  $\text{MoS}_2$  magnetron-sputtered on candle soot for enhanced hydrogen evolution reaction. *Appl Catal B* 263:117750. <https://doi.org/10.1016/j.apcatb.2019.117750>
- [18] Sun H, Yan Z, Liu F, Xu W, Cheng F, Chen J (2020) Self-supported transition-metal-based electrocatalysts for hydrogen and oxygen evolution. *Adv Mater* 32:1806326. <https://doi.org/10.1002/adma.201806326>
- [19] Li J-S, Zhang S, Sha J-Q, Wang H, Liu MZ, Kong L-X, Liu G-D (2018) Confined molybdenum phosphide in P-doped porous carbon as efficient electrocatalysts for hydrogen evolution. *ACS Appl Mater Interfaces* 10:17140. <https://doi.org/10.1021/acsami.8b01541>
- [20] Li J-S, Li J-Y, Wang X-R, Zhang S, Sha J-Q, Liu G-D (2018) Reduced graphene oxide-supported MoP@P-doped porous carbon nano-octahedrons as high-performance electrocatalysts for hydrogen evolution. *ACS Sustain Chem Eng* 6:10252. <https://doi.org/10.1021/acssuschemeng.8b01575>
- [21] Hou Y, Pang H, Zhang L et al (2020) Highly dispersive bimetallic sulfides afforded by crystalline polyoxometalate-based coordination polymer precursors for efficient hydrogen evolution reaction. *J Power Sour* 446:227319. <https://doi.org/10.1016/j.jpowsour.2019.227319>
- [22] Xia W, Qu C, Liang Z et al (2017) High-performance energy storage and conversion materials derived from a single metal-organic framework/graphene aerogel composite. *Nano Lett* 17:2788–2795. <https://doi.org/10.1021/acs.nanolett.6b05004>
- [23] Dempsey JL, Brunschwig BS, Winkler JR, Gray HB (2009) Hydrogen evolution catalyzed by cobaloximes. *ACC Chem Res* 42:1995–2004. <https://doi.org/10.1021/ar900253e>
- [24] Artero V, Chavarot-Kerlidou M, Fontecave M (2011) Splitting water with cobalt. *Angew Chem Int Ed* 50:7238–7266. <https://doi.org/10.1002/anie.201007987>
- [25] Baffert C, Artero V, Fontecave M (2007) Cobaloximes as functional models for hydrogenases. 2. Proton electroreduction catalyzed by difluoroborylbis (dimethylglyoximate) cobalt (II) complexes in organic media. *Inorg Chem* 46:1817–1824. <https://doi.org/10.1021/ic061625m>
- [26] Jacques P-A, Artero V, Pécaut J, Fontecave M (2009) Cobalt and nickel diimine-dioxime complexes as molecular electrocatalysts for hydrogen evolution with low overvoltages. *PNAS* 106:20627–20632. <https://doi.org/10.1073/pnas.0907775106>
- [27] Fourmond V, Jacques P-A, Fontecave M, Artero V (2010)  $\text{H}_2$  evolution and molecular electrocatalysts: determination of overpotentials and effect of homoconjugation. *Inorg Chem* 49:10338–10347. <https://doi.org/10.1021/ic101187v>
- [28] Zhang K, Xia X, Deng S et al (2019) N-doped CoO nanowire arrays as efficient electrocatalysts for oxygen evolution reaction. *J Energy Chem* 37:13–17. <https://doi.org/10.1016/j.jechem.2018.11.013>
- [29] Lee C-P, Chen W-F, Billo T et al (2016) Beaded stream-like  $\text{CoSe}_2$  nanoneedle array for efficient hydrogen evolution electrocatalysis. *J Mater Chem A* 4:4553–4561. <https://doi.org/10.1039/c6ta00464d>
- [30] Zheng Y-R, Gao M-R, Yu Z-Y, Gao Q, Gao H-L, Yu S-H (2015) Cobalt diselenide nanobelts grafted on carbon fiber felt: an efficient and robust 3D cathode for hydrogen production. *Chem Sci* 6:4594–4598. <https://doi.org/10.1039/c5sc01335f>
- [31] Sun C, Dong Q, Yang J et al (2016) Metal-organic framework derived  $\text{CoSe}_2$  nanoparticles anchored on carbon fibers as bifunctional electrocatalysts for efficient overall water splitting. *Nano Res* 9:2234–2243. <https://doi.org/10.1007/s12274-016-1110-1>
- [32] Xue N, Lin Z, Li P, Diao P, Zhang Q (2020) Sulfur-doped  $\text{CoSe}_2$  porous nanosheets as efficient electrocatalysts for the hydrogen evolution reaction. *ACS Appl Mater Interfaces* 12:28288–28297. <https://doi.org/10.1021/acsami.0c07088>
- [33] Wang H, Min S, Wang Q et al (2017) Nitrogen-doped nanoporous carbon membranes with Co/CoP janus-type nanocrystals as hydrogen evolution electrode in both acidic and alkaline environments. *ACS Nano* 11:4358–4364. <https://doi.org/10.1021/acsnano.7b01946>
- [34] Xu M, Han L, Han Y, Yu Y, Zhai J, Dong S (2015) Porous CoP concave polyhedron electrocatalysts synthesized from metal-organic frameworks with enhanced electrochemical

- properties for hydrogen evolution. *J Mater Chem A* 3:21471–21477. <https://doi.org/10.1039/c5ta05018a>
- [35] Li J-S, Kong L-X, Wu Z, Zhang S, Yang X-Y, Sha J-Q, Liu G-D (2019) Polydopamine-assisted construction of cobalt phosphide encapsulated in N-doped carbon porous polyhedrons for enhanced overall water splitting. *Carbon* 145:694. <https://doi.org/10.1016/j.carbon.2018.12.032>
- [36] Zhu D, Zhen Q, Xin J, Ma H, Tan L, Pang H, Wang X (2020) A free-standing and flexible phosphorus/nitrogen dual-doped three-dimensional reticular porous carbon frameworks encapsulated cobalt phosphide with superior performance for nitrite detection in drinking water and sausage samples. *Sens Actuators B* 321:128541. <https://doi.org/10.1016/j.snb.2020.128541>
- [37] Caban-Acevedo M, Stone ML, Schmidt JR, Thomas JG, Ding Q, Chang H-C, Tsai M-L, He J-H, Jin S (2015) Efficient hydrogen evolution catalysis using ternary pyrite-type cobalt phosphosulphide. *Nat Mater* 14:1245–1251. <https://doi.org/10.1038/nmat4410>
- [38] Sun X, Huang H, Wang C, Liu Y, Hu T-L, Bu X-H (2018) Effective  $\text{Co}_x\text{S}_y$  hetero electrocatalysts fabricated by in-situ sulfuration of a metal-organic framework. *Chem ElectroChem* 5:3639–3644. <https://doi.org/10.1002/celec.201801238>
- [39] Guo Y, Zhang R, Hao W, Zhang J, Yang Y (2020) Multifunctional Co-B-O@ $\text{Co}_x\text{B}$  catalysts for efficient hydrogen generation. *Int J Hydrogen Energy* 45:380–390. <https://doi.org/10.1016/j.ijhydene.2019.09.008>
- [40] Kuang M, Wang Q, Han P, Zheng G (2017) Cu, Co-embedded n-enriched mesoporous carbon for efficient oxygen reduction and hydrogen evolution reactions. *Adv Energy Mater* 7:1700193. <https://doi.org/10.1002/aenm.201700193>
- [41] Zhou J, Yu L, Zhou Q, Huang C, Zhang Y, Yu B, Yu Y (2021) Ultrafast fabrication of porous transition metal foams for efficient electrocatalytic water splitting. *Appl Catal B* 288:120002. <https://doi.org/10.1016/j.apcatb.2021.120002>
- [42] Anantharaj S, Ede SR, Sakthikumar K, Karthick K, Mishra S, Kundu S (2016) Recent trends and perspectives in electrochemical water splitting with an emphasis on sulfide, selenide, and phosphide catalysts of Fe Co, and Ni: a review. *ACS Catal* 6:8069–8097. <https://doi.org/10.1021/acscatal.6b02479>
- [43] Chen J, Xia G, Jiang P et al (2016) Active and durable hydrogen evolution reaction catalyst derived from Pd-doped metal-organic frameworks. *ACS Appl Mater Interfaces* 8:13378–13383. <https://doi.org/10.1021/acsami.6b01266>
- [44] Huang B, Chen L, Wang Y, Ouyang L, Ye J (2017) Paragenesis of palladium-cobalt nanoparticle in nitrogen-rich carbon nanotubes as bifunctional electrocatalyst for hydrogen evolution reaction and oxygen reduction reaction. *Chemistry* 23:7710–7718. <https://doi.org/10.1002/chem.201700544>
- [45] Du N, Wang C, Long R, Xiong Y (2017) N-doped carbon-stabilized PtCo nanoparticles derived from Pt@ZIF-67: highly active and durable catalysts for oxygen reduction reaction. *Nano Res* 10:3228–3237. <https://doi.org/10.1007/s12274-017-1611-6>
- [46] Li J-S, Huang M-J, Chen X-N et al (2020) Synergistically enhanced hydrogen evolution reaction by ruthenium nanoparticles dispersed on N-doped carbon hollow nanospheres. *Chem Commun* 56:6802. <https://doi.org/10.1039/D0CC01765E>
- [47] Kitchin JR, Nørskov JK, Barteau MA, Chen J (2004) Role of strain and ligand effects in the modification of the electronic and chemical properties of bimetallic surfaces. *Phys Rev Lett* 93:156801. <https://doi.org/10.1103/PhysRevLett.93.156801>
- [48] Zheng Y, Jiao Y, Jaroniec M, Qiao SZ (2015) Advancing the electrochemistry of the hydrogen-evolution reaction through combining experiment and theory. *Angew Chem Int Ed* 54:52–65. <https://doi.org/10.1002/anie.201407031>
- [49] Tabassum H, Guo W, Meng W, Mahmood A, Zhao R, Wang Q, Zou R (2017) Metal-organic frameworks derived cobalt phosphide architecture encapsulated into B/N co-doped graphene nanotubes for all pH value electrochemical hydrogen evolution. *Adv Energy Mater* 7:1601671. <https://doi.org/10.1002/aenm.201601671>
- [50] Wang T, Zhou Q, Wang X, Zheng J, Li X (2015) MOF-derived surface modified Ni nanoparticles as an efficient catalyst for the hydrogen evolution reaction. *J Mater Chem A* 3:16435–16439. <https://doi.org/10.1039/c5ta04001a>
- [51] Zhang J, Bai T, Huang H, Yu M-H, Fan X, Chang Z, Bu X-H (2020) Metal-organic-framework-based photocatalysts optimized by spatially separated cocatalysts for overall water splitting. *Adv Mater* 32:2004747. <https://doi.org/10.1002/adma.202004747>
- [52] Kong L, Zhong M, Shuang W, Xu Y, Bu X-H (2020) Electrochemically active sites inside crystalline porous materials for energy storage and conversion. *Chem Soc Rev* 49:2378–2407. <https://doi.org/10.1039/c9cs00880b>
- [53] Liu M, Kong L, Wang X, He J, Bu X-H (2019) Engineering bimetal synergistic electrocatalysts based on metal-organic frameworks for efficient oxygen evolution. *Small* 15:1903410. <https://doi.org/10.1002/smll.201903410>
- [54] Wang C-P, Liu H-Y, Bian G et al (2019) Metal-layer assisted growth of ultralong quasi-2D mof nanoarrays on arbitrary substrates for accelerated oxygen evolution. *Small* 15:1906086. <https://doi.org/10.1002/smll.201906086>
- [55] Wang X, Feng Z, Xiao B et al (2020) Polyoxometalate-based metal-organic framework-derived bimetallic hybrid

- materials for upgraded electrochemical reduction of nitrogen. *Green Chem* 22:6157. <https://doi.org/10.1039/D0GC01149E>
- [56] Yang J, Zhang F, Lu H, Hong X, Jiang H, Wu Y, Li Y (2015) Hollow Zn/Co ZIF particles derived from core-shell ZIF-67@ZIF-8 as selective catalyst for the semi-hydrogenation of acetylene. *Angew Chem Int Ed* 54:10889–10893. <https://doi.org/10.1002/anie.201504242>
- [57] Zhong M, Zhang X, Zhao B, Yang D, Xie Z, Zhou Z, Bu X-H (2017) Zeolitic imidazole framework derived composites of nitrogen-doped porous carbon and reduced graphene oxide as high-efficiency cathode catalysts for Li-O<sub>2</sub> batteries. *Inorg Chem Front* 4:1533–1538. <https://doi.org/10.1039/c7qi00314e>
- [58] Wang S, Wang J, Zhu M et al (2015) Molybdenum-carbide-modified nitrogen-doped carbon vesicle encapsulating nickel nanoparticles: a highly efficient, low-cost catalyst for hydrogen evolution reaction. *J Am Chem Soc* 137:15753. <https://doi.org/10.1021/jacs.5b07924>
- [59] Xue H, Tang J, Gong H et al (2016) Fabrication of PdCo bimetallic nanoparticles anchored on three-dimensional ordered n-doped porous carbon as an efficient catalyst for oxygen reduction reaction. *ACS Appl Mater Interfaces* 8:20766–20771. <https://doi.org/10.1021/acsami.6b05856>
- [60] Artyushkova K, Kiefer B, Halevi B, Knop-Gericke A, Schlögl R, Atanassov P (2013) Density functional theory calculations of XPS binding energy shift for nitrogen-containing graphene-like structures. *Chem Commun* 49:2539–2541. <https://doi.org/10.1039/c3cc40324f>
- [61] Wang AL, He XJ, Lu XF, Xu H, Tong YX, Li GR (2015) Palladium-cobalt nanotube arrays supported on carbon fiber cloth as high-performance flexible electrocatalysts for ethanol oxidation. *Angew Chem Int Ed* 54:3669–3673. <https://doi.org/10.1002/anie.201410792>
- [62] Maheswari S, Karthikeyan S, Murugan P, Sridhar P, Pitchumani S (2012) Carbon-supported Pd-Co as cathode catalyst for APEMFCs and validation by DFT. *Phys Chem Chem Phys* 14:9683–9695. <https://doi.org/10.1039/c2cp40655a>
- [63] Zou X, Zhang Y (2015) Noble metal-free hydrogen evolution catalysts for water splitting. *Chem Soc Rev* 44:5148–5180. <https://doi.org/10.1039/C4CS00448E>

**Publisher's Note** Springer Nature remains neutral with regard to jurisdictional claims in published maps and institutional affiliations.